

Supporting Information

for

Elucidating the Drug Release from Metal-Organic Framework Nanocomposites *via in situ* Synchrotron Microspectroscopy and Theoretical Modelling

Barbara E. Souza,^a Lorenzo Donà,^b Kirill Titov,^a Paolo Bruzzese,^b Zhixin Zeng,^a Yang Zhang,^a Arun S. Babal,^a Annika F. Möslein,^a Mark D. Frogley,^c Magda Wolna,^c Gianfelice Cinque,^c Bartolomeo Civalleri,^{*b} and Jin-Chong Tan^{**a}

^a*Multifunctional Materials & Composites (MMC) Laboratory, Department of Engineering Science, University of Oxford, Parks Road, Oxford OX1 3PJ, UK*

^b*Department of Chemistry, NIS and INSTM Reference Centre, University of Turin, via Pietro Giuria 7, Torino 10125, Italy*

^c*Diamond Light Source, Harwell Campus, Chilton, Oxford OX11 0DE, United Kingdom*

**bartolomeo.civalleri@unito.it*

***jin-chong.tan@eng.ox.ac.uk*

Contents

1. Methods.....	2
2. Synchrotron radiation Fourier transform infrared microspectroscopy (SR-microFTIR).....	5
3. Thermogravimetric analysis (TGA).....	9
4. Atomic force microscopy (AFM) and scanning electron microscopy (SEM).....	11
5. Understanding SR-microFTIR data <i>via</i> DFT calculations.....	13
6. Density functional theory (DFT) calculations	17
7. Powder X-ray diffraction (PXRD) patterns	24
8. Water accessibility in MOF/PU composites	25
9. Analysis of synchrotron microFTIR data.....	28
References	29

1. Methods

MOF synthesis. The HKUST-1 particles (crystal size from 50-300 nm) were synthesized *via* a manual grinding process. $\text{Cu}(\text{NO}_3)_2 \cdot 3\text{H}_2\text{O}$ [copper(II) nitrate trihydrate] (1.5 mmol) and H_3BTC [benzene-1,3,5-tricarboxylic acid] (1.0 mmol) were combined in the agate mortar and manually ground for 10 min. The product was washed with methanol and separated by centrifugation (8000 rpm for 10 min). 5-FU@HKUST-1 powder sample was synthesized *via* an *in situ* encapsulation methodology (one-pot synthesis). Analogous procedure to the synthesis of pristine HKUST-1 was followed with the addition of 3.5 mmol of 5-FU during the grinding process. Pristine HKUST-1 and drug-loaded sample were washed by centrifugation (8000 rpm for 10 min) with methanol, dried at room temperature, and finally activated at 90 °C for 12 h in a vacuum oven. After synthesis, HKUST-1 and 5-FU@HKUST-1 powder samples, together with 5-FU powder (used as acquired from Fisher Scientific, UK), were dispersed in methanol and drop casted onto the ZnSe window (substrate) for synchrotron radiation microFTIR measurements.

MOF/Polymeric composite preparation. Polyurethane (PU) solution was prepared by dissolving poly [4,4'-methylenebis(phenyl isocyanate)-alt-1,4-butanediol/di(propylene glycol)/polyurethane] pellets (purchased from Sigma Aldrich and used without further alterations) in tetrahydrofuran (THF) for 24-48 hours until complete dissolution of polymer pellets. 85 wt.% MOF/PU composites integrating 5-FU@HKUST-1, HKUST-1 (corresponding to wt.% Eq.1) and pristine PU composites were produced by dispersion of a certain amount of previously synthesized MOF particles in a small amount of THF (30 mg of MOF per 1 mL of THF) before their incorporation into the PU-THF solution. The dispersion was performed by a combination of sonication (5 min) and magnetic stirring (20 min, 80 rpm). 14 wt.% 5-FU/PU membrane was produced by following an analogous procedure. This strategy, reported by Cohen *et al.*³³, has proven to be a versatile approach for the preparation of homogeneous MOF/polymer composites. Subsequently the membranes were fabricated by drop casting the solution onto the substrates (one drop of ~40 μL), inclined at an angle of 60°, allowing it to flow until the edge of the substrate. The drop casting procedure was done at room temperature with subsequent evacuation of samples at 65 °C for the removal of remaining solvents.

$$\text{MOF wt. \%} = \left(\frac{m_{\text{MOF}}}{m_{\text{MOF}} + m_{\text{PU}}} \right) \times 100\% \quad (1)$$

where m_{MOF} is the weight of MOF nanoparticles (dispersed in THF) and m_{PU} is the weight of PU (pellets dissolved in THF).

Synchrotron radiation Fourier transform infrared microspectroscopy. SR-microFTIR spectra were acquired in Beamline B22 MIRIAM at the Diamond Light Source (Oxfordshire, UK). The spectra were collected in transmission mode by employing an infrared microscope (Bruker Hyperion 3000)

equipped with a 36× objective lens, from spot areas delimited by the IR microscope slits comprising a ~10×10 μm square. The spectra of different regions in the sample were collected in the mid-IR region encompassing the broad spectral range of ~650-4000 cm⁻¹, using a spectral resolution of 4 cm⁻¹ and 256 scans resulting in ~40 s per spectrum. Two key experiments have been carried out with different variations of the *in situ* experimental setup. Because of the difference in the frequency of the bending modes of deionized water (H₂O) and deuterated water (D₂O) and the overlap of these modes with important vibrational bands of the drug molecule present in the drug@MOF samples, the monitoring of drug release was carried out with a combination of experiments performed in H₂O and D₂O to fully establish the evolution of drug peaks within the broad spectral range.

Static cell. For static cell SR-microFTIR measurements, powder and polymer composite samples were loaded into a customized liquid cell, sandwiched between two zinc selenide (ZnSe) circular windows (1 mm thickness, ø = 25 mm) separated by a 10-μm thick Teflon spacer. Liquid measurements were conducted with the addition of 2 μL of deuterated water (D₂O), placed within the cell confinement. The sample under study was only partially in contact with D₂O in order to enable the collection of dry and wet backgrounds as reference spectra. Data was collected in the range of 650-4000 cm⁻¹, at a resolution of 4 cm⁻¹.

Flow cell. A range of pre-experimental tests were performed in order to optimize the use of the dynamic flow cell to enable SR-microFTIR measurements. Samples were loaded into a demountable liquid cell sandwiched between two ZnSe circular windows (2-mm thick, ø = 25 mm), separated by a 10-μm thick gold spacer. Measurements were performed with provision for medium exchange (D₂O and deionized water (H₂O)) *via* an automatic syringe pump. A flow-rate of 100 μL min⁻¹ was used to fully replace media in the sample chamber throughout the experiment. For measurement in D₂O flow, the media were allowed to flow for approximately 25 minutes before starting data collection, thus allowing the system to reach D-H equilibrium. The enhanced magnification allowed data collection in a 10×10 μm scanning window, obtaining good signal-to-noise through the aqueous media. Data were collected in the range of 650-4000 cm⁻¹, at a resolution of 4 cm⁻¹. The dynamic flow study permitted us to collect over 180 individual IR spectra at different timepoints, over a period of ~2 hours. By taking advantage of the possibility to maintain sample to media contact for long periods of time in the flow environment, we acquired spectra with high signal-to-noise ratio and excellent spectral quality.

SR-microFTIR data processing. Pre-processing of spectral data was performed using the OPUS software version 7.2 (Bruker Optics). FTIR spectra was initially truncated to separate the spectral region of 700-1800 cm⁻¹. “Concave rubberband correction” from the OPUS software was applied with 4000 points followed by max-min normalization in the range of 1680-1760 cm⁻¹ (polyurethane peak).

Ab initio density functional theory (DFT) calculations. DFT calculations of HKUST-1 and its complexes with 5-FU (*i.e.* 5-FU@HKUST-1 adducts A-D) and water were performed using the *ab initio* periodic code CRYSTAL17.²² We employed the PBEsol0-3c composite method recently devised for cost effective solid state calculations.²³ For all calculations we referred to a ferromagnetic unit cell. Model structures were fully optimized by means of an unconstrained relaxation of both lattice parameters and atomic positions. Interaction energies were computed through a supermolecule approach and for adduct A and D they were validated against the more costly benchmark Becke, 3 parameter, Lee Yang Parr (B3LYP) method^{34,35} augmented with the D3 dispersion correction including two- and three-body terms³⁶ and combined with a VTZP basis set³⁷ (*i.e.* B3LYP-D3(ABC)/VTZP). Because of the good tradeoff between cost and accuracy of the PBEsol-3c method, vibrational frequencies at the Γ point and their IR intensities were calculated on the optimized geometry by means of a mass-weighted Hessian matrix, obtained by numerical differentiation of the analytical nuclear gradients with a three-point formula.^{38,39} The Pack-Monkhorst/Gilat shrinking factors for the reciprocal space sampling were set to 2, corresponding to 6 to 8 k-points at which the Hamiltonian matrix was diagonalized. The condition for the SCF convergence was set to 10^{-8} and 10^{-10} Hartrees during structure optimization and vibrational frequency calculations, respectively.

Powder X-ray diffraction. PXRD patterns of powder and composite samples were collected using the Rigaku MiniFlex diffractometer with a Cu K α source (1.541 Å). Diffraction data were collected from 3° to 30°, using a 0.02° step size and 1.0° min⁻¹ step speed. The patterns were then normalized with respect to the most intense peak and used for phase identification, except for decomposition studies in which the absolute intensity was used to analyze the decomposition of materials.

Scanning electron microscope and atomic force microscope. Analyses of the surface topography of the membranes was carried out by scanning electron microscopy (SEM) and atomic force microscopy (AFM). SEM images were obtained using Carl Zeiss EVO LS15 at 15 keV under high vacuum. Atomic force microscopy (AFM) was performed using the Veeco Dimension 3100 AFM under the tapping mode, equipped with a Tap300G silicon probe with a resonance frequency of 30 kHz (spring constant 40 Nm⁻¹, tip radius < 10 nm).

Thermogravimetric analysis. Thermogravimetric analysis (TGA) of the samples was performed using TGA-Q50 (TA instruments). Approximately 4 mg of each sample were placed in a platinum pan (maximum volume 50 μ L) and heated from 50 °C to 500 °C. The measurements were performed at a heating rate of 10 °C min⁻¹ and under a dry nitrogen flow of 40 mL min⁻¹.

Calculation of integrated spectral area. The Integrate Gadget in OriginPro software was used to perform the numerical integration on the FTIR spectra and determine the area under the curve of specific vibrational modes. The range of data was selected to include the peaks of the vibrational modes of

interest, using the (horizontal) wavenumber axis as the baseline. To facilitate the comparison across different samples, the area values were normalized against its initial area value.

Contact angle measurements. Contact angle measurements were performed by the addition of small droplets of deionized water (10 μL) on top of HKUST-1/PU and PU membranes. A monochrome CMOS camera ($6\times 6 \mu\text{m}^2$) integrated with a Navitar 12 \times zoom lens was used to obtain images used for the measurements. ImageJ software was then applied to compute the contact angle values.

Swelling experiments. Swelling behavior of composites was measured by a gravimetric method. HKUST-1/PU and PU membranes were immersed in deionized water at room temperature until the swelling equilibrium was reached. Samples were removed and blotted with filter paper to remove the excess water on the surface, and then weighed. The immersion time and drying procedure were repeated until the weight of the swollen samples became constant. The swelling ratio and the swelling water content as a percentage were defined by Eq. 2:

$$\text{Swelling ratio \%} = \left(\frac{m_{\text{swollen}} - m_{\text{dry}}}{m_{\text{dry}}} \right) \times 100\% \quad (2)$$

where m_{swollen} is the mass of the sample after immersion in water and m_{dry} is the mass of the initially dry sample.

2. Synchrotron radiation Fourier transform infrared microspectroscopy (SR-microFTIR)

Table S1. Samples description and details

	Sample	Synthesis method	Details
Powder samples	HKUST-1	Manual grinding	Pristine MOF
	5-FU@HKUST-1	Manual grinding	<i>In situ</i> encapsulation
	5-FU	-	As-received
Polymer composites samples	HKUST-1/PU	Drop cast	85 wt.% / 15 wt.%
	5-FU@HKUST-1/PU	Drop cast	85 wt.% / 15 wt.%
	HKUST-1/PU	Drop cast	85 wt.% / 15 wt.%
	5-FU/PU	Drop cast	14 wt.% / 86 wt.%

The concentrations presented in Table S1 were chosen so that the concentration of 5-FU present in 5-FU/PU composite was compatible with the amount of 5-FU present in the 5-FU@HKUST-1/PU composite (as determined by thermogravimetric analysis, presented later in this Supporting Information).

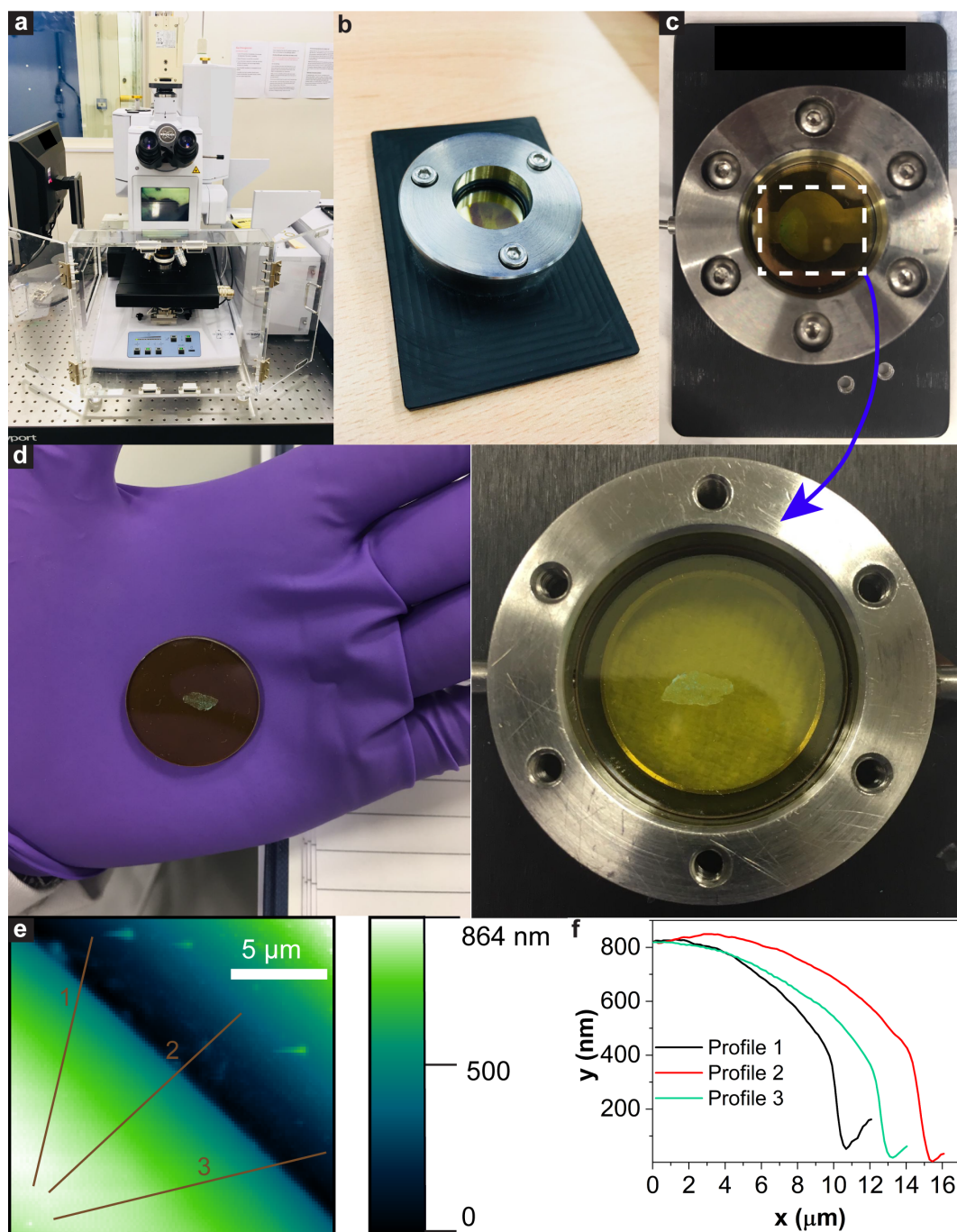


Figure S1. Experimental setup for *in situ* SR-microFTIR spectroscopy measurements. (a) Optics FTIR microscope. (b) Static liquid cell. (c) Flow liquid cell. (d) Sample deposition onto a pair of 25-mm diameter zinc selenide (ZnSe) circular windows. During the experiments, the samples remained fully attached to the ZnSe windows, as a result of the drop cast technique applied for their fabrication. (e) AFM image of membrane produced *via* drop casting. Profiles presented in (f) show that the thickness of the membranes was less than 1 μm .

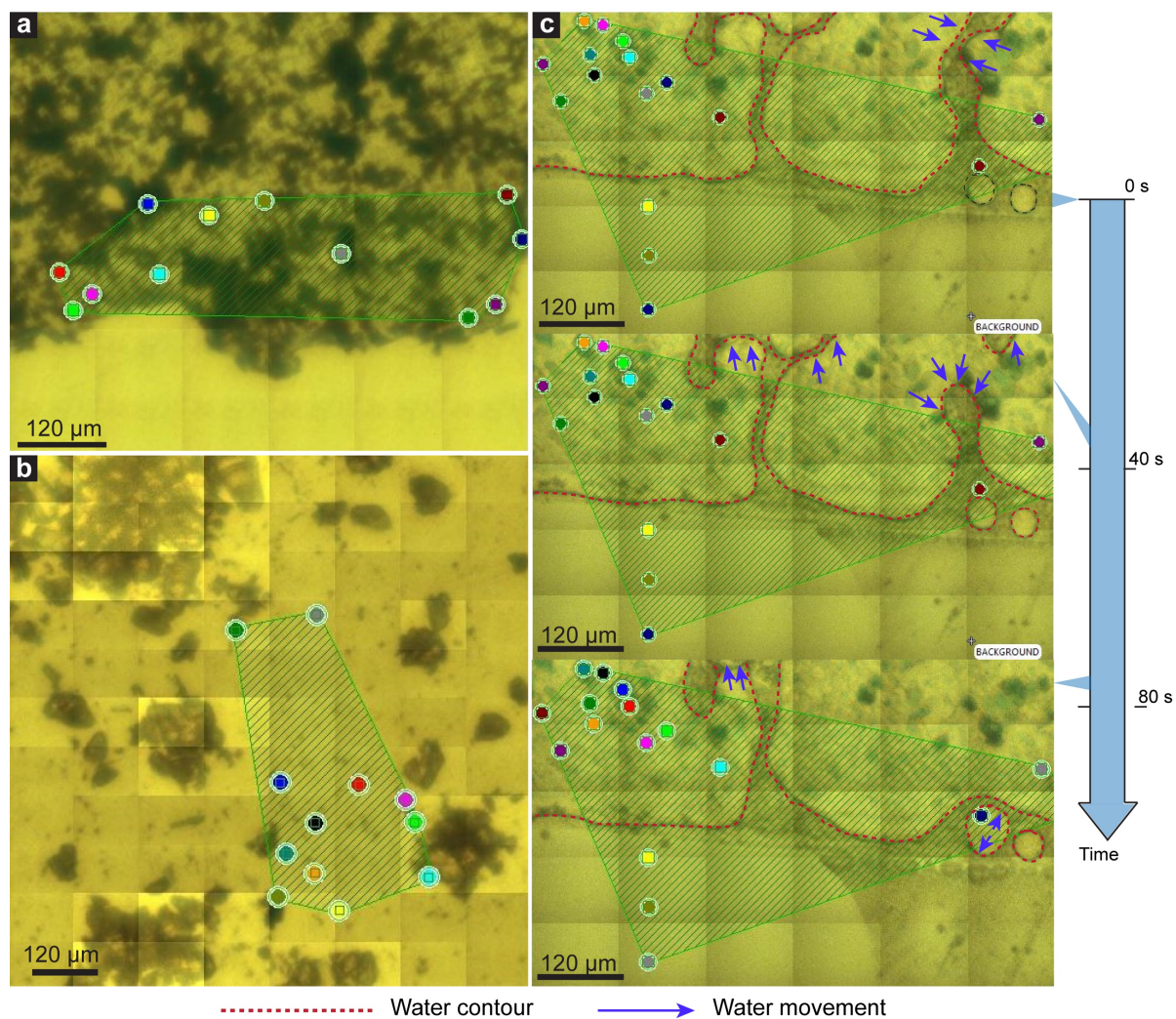


Figure S2. Optical micrographs showing multiple sites selected in the samples for extensive data acquisition. (a) HKUST-1/PU membrane, (b) 5-FU crystals, and (c) 5-FU@HKUST-1/PU membrane in contact with water. The movement of the medium can be observed by contrasting the images c-top to c-bottom.

2.1. Media – HKUST-1 interaction

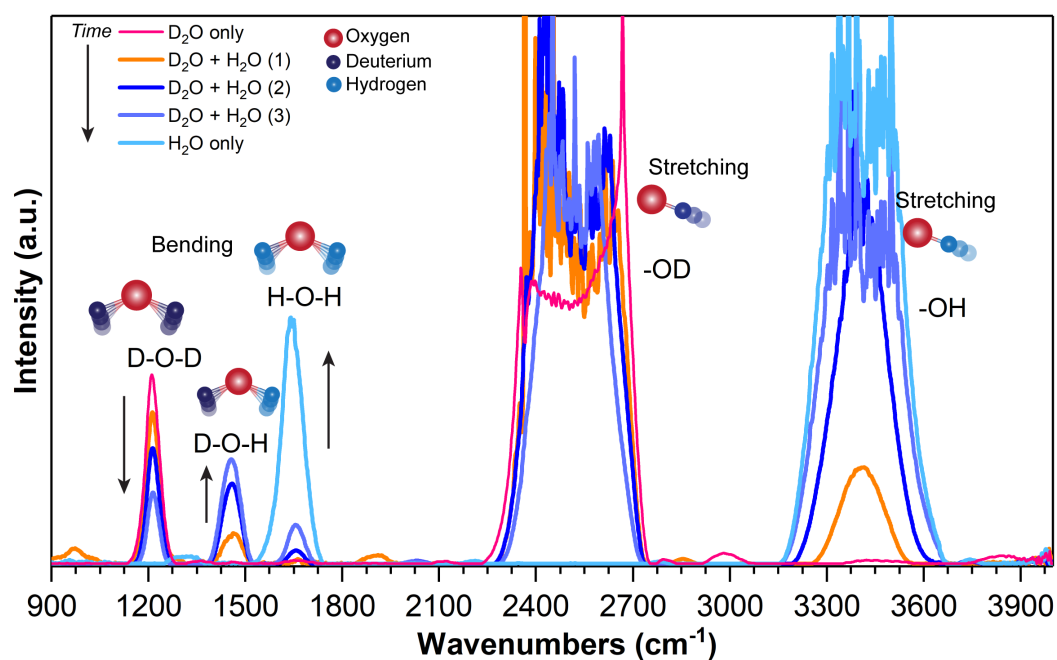


Figure S3. SR-microFTIR spectra of deionized water (H_2O) and deuterated water (D_2O). Specific bending and stretching modes are illustrated. Observe the saturation of $-\text{OD}$ and $-\text{OH}$ stretching bands due to the high signal of solvent in the range $> 2000 \text{ cm}^{-1}$.

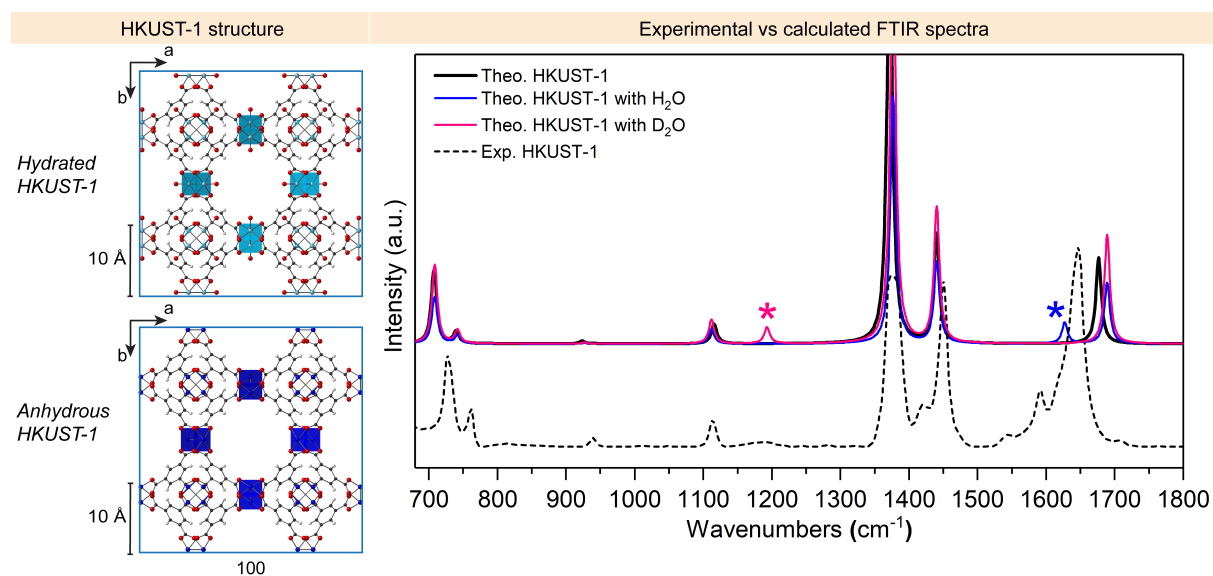


Figure S4. Theoretical spectra of activated and hydrated HKUST-1 (H_2O -HKUST-1 and D_2O -HKUST-1). The comparison between the spectra shows the respective bending modes of D_2O and H_2O (observed in the experimental spectra) when coordinated to the copper sites in HKUST-1. A scaling factor of 0.95 was applied to the theoretical spectra eliminate common shifts resulting from the *ab initio* calculations and match the frequencies against the experimental spectrum. Colour code: O in red, C in black, H in grey, hydrated Cu in light blue, and activated Cu in navy blue.

3. Thermogravimetric analysis (TGA)

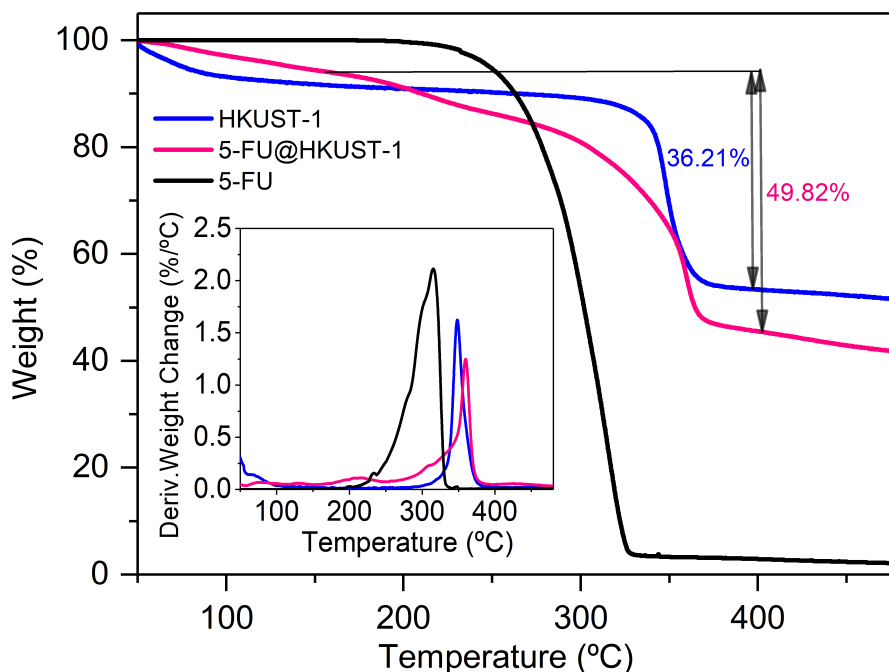


Figure S5. TGA of HKUST-1 (blue), 5-FU@HKUST-1 (pink), and 5-FU (black) samples with inset showing the derivative weight change with respect to temperature. Inset shows the differential material decomposition behaviour as a function of temperature.

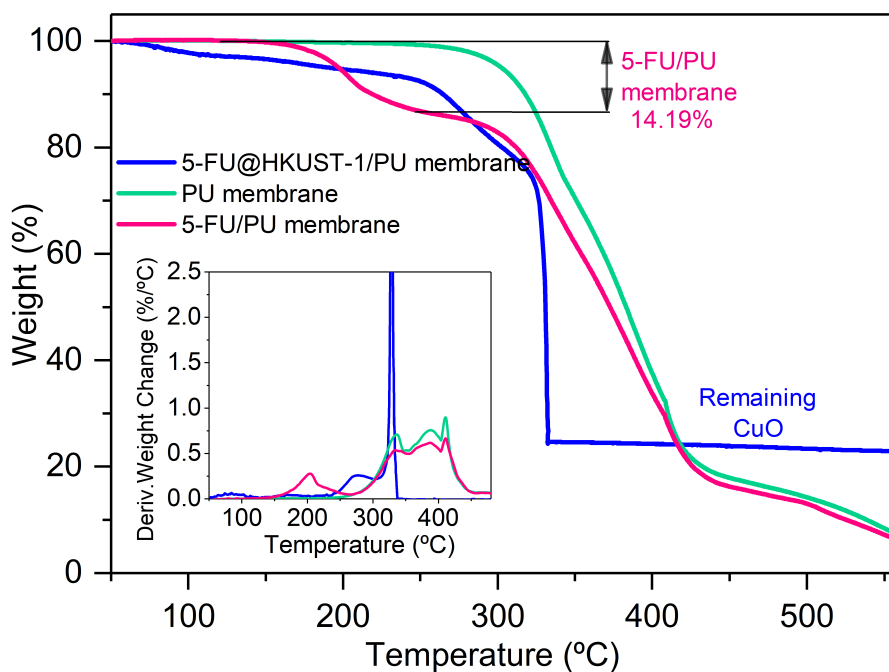


Figure S6. TGA of PU membrane (green) versus 5-FU@HKUST-1/PU (blue) and 5-FU/PU membrane (pink) and samples. Insets display the derivative weight change with respect to the temperature.

Table S2 displays the drug loading (wt.%) of different 5-FU@MOFs compared to other potential carriers of 5-FU. The loadings varied from 1.9 wt.% to 69.7 wt.%, being the loading achieved in our 5-FU@HKUST-1 in good agreement with what has been achieved in recent works. It is worth noting that most of the 5-FU@MOF systems presented in Table S2 used conventional immersion/impregnation encapsulation technique in which the carrier was immersed into a 5-FU solution for different periods of time. However, our *in situ* technique reported herein is different from the reported literature approach, by ensuring that the drug molecules were not attached to the external wall of the host carrier.

Table S2. Comparison of 5-FU loading employing different MOF hosts.

	MOF	5-FU loading (wt. %)	Reference	
Copper MOFs	HKUST-1	14.0	This work	2019
	Cu-MOF	17.3	¹	2018
	Cu-MOF	47.3	²	2018
	HKUST-1	40.2	³	2017
Various MOF systems	ZIF-8	5.0	⁴	2020
	In-MOF	32.6	⁵	2019
	Gd-MOF	47.0	⁶	2019
	Zn-MOF	36.8	⁷	2018
	Dy-MOF	20.6	⁸	2018
	Nd-MOF	18.0	⁹	2016
	CD-MOF-1	15.7	¹⁰	2018
	MIL-53(Fe)	13.1		
	MIL-88(Fe)	28.0	¹¹	2018
	MIL-100(Fe)	66.0		
Conventional DDS	Zn-MOF	44.8	¹²	2018
	FeO nanoparticles	1.9	¹³	2018
	Chitosan nanoparticles	29.9-69.7	¹⁴	2012
	Polysaccharides particles	3.0	¹⁵	2008

4. Atomic force microscopy (AFM) and scanning electron microscopy (SEM)

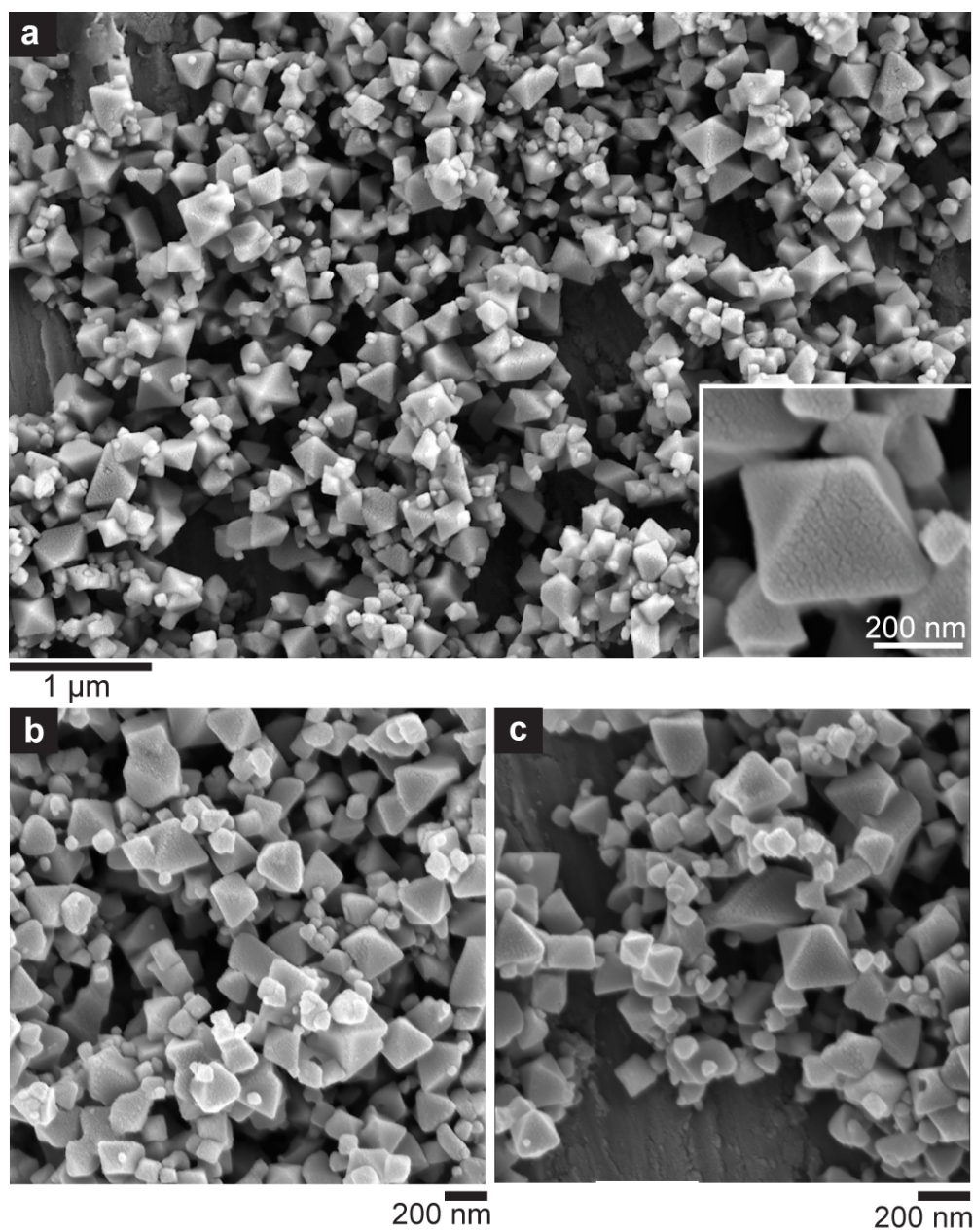


Figure S7. SEM micrographs of as synthesized (a-b) pristine HKUST-1 (crystal size = 432 ± 83 nm (averaged of 100 measurements)), and (c) 5-FU@HKUST-1 (crystal size = 421 ± 75 nm (averaged of 100 measurements)). Note the non-uniform crystal size distribution varying from *ca.* 50 to 500 nm.

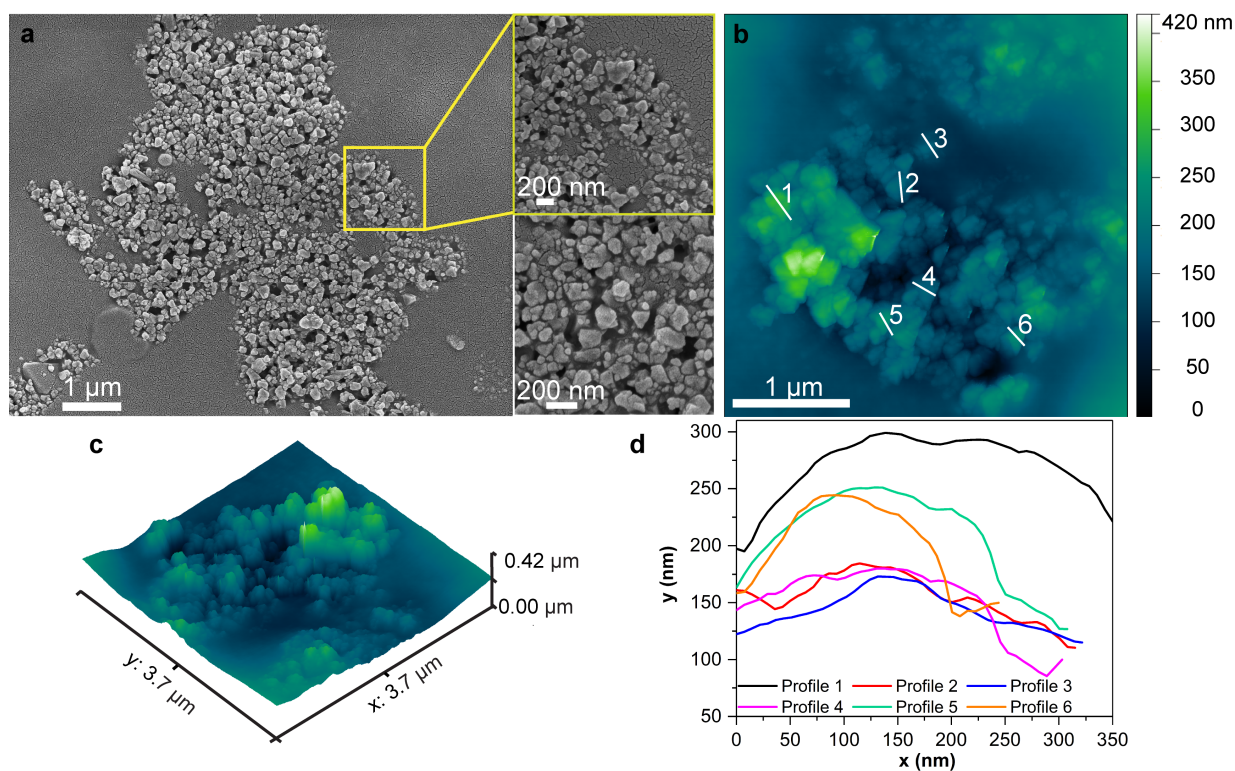


Figure S8. SEM and AFM micrographs of membranes produced for the SR-microFTIR experiments. (a) SEM of pristine HKUST-1 crystal embedded in the PU matrix. Zoom-ins show details of the membrane where HKUST-1 particles are coated by the polymer. (b) AFM image of HKUST-1/PU membrane for morphology characterization, accompanied by (c) 3D representation of the surface topography. (d) Height profiles from traces marked in (b). The smooth edges demonstrate the coating of the crystals by the polymer.

5. Understanding SR-microFTIR data *via* DFT calculations

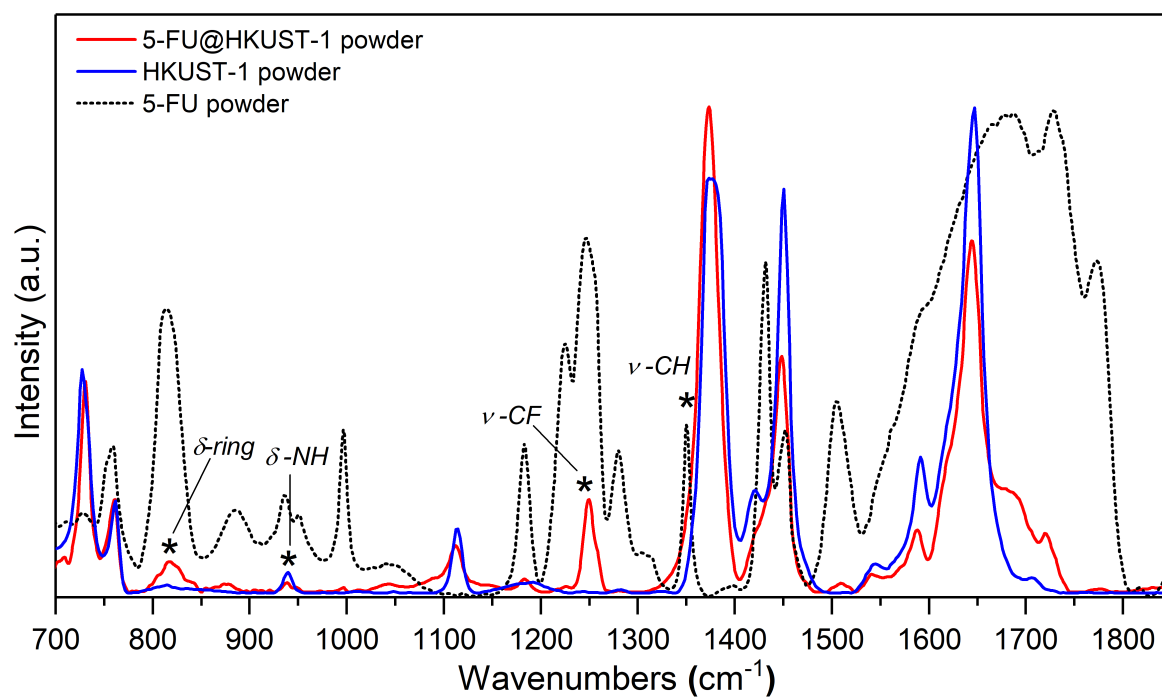


Figure S9. SR-microFTIR spectra of 5-FU@HKUST-1, HKUST-1, and 5-FU powder samples collected using the static fluid-cell. The asterisks denote the vibrations of 5-FU guest molecules detected in the 5-FU@HKUST-1 sample.

Table S3: Details of main vibrational bands of the HKUST-1 framework, 5-FU guest and PU polymer matrix

	Exp. (cm ⁻¹)	Description
HKUST-1	1646	Asymmetric COO stretching
	1590	Symmetric COO stretching
	1450	Asymmetric COO stretching
	1374	Symmetric COO stretching
	759	Out-of-plane C–H bending of benzene ring
	729	
H ₂ O	1617	Bending of molecular water (Modes appear when H ₂ O is coordinated to the copper site)
5-FU ¹⁶	1686	C=C bending
	1452	N–H bending
	1430	Stretching of ring
	1350	C–H stretching
	1279	C–F stretching
	1184	In-plane N–H bending
	959	
	883	Out-of-plane C–H bending
	814	Ring deformation
	757	
PU ^{17,18}	1732	C=O stretching
	1532	N–H bending
	1230	C–N bending
	1080	C–O–C bending

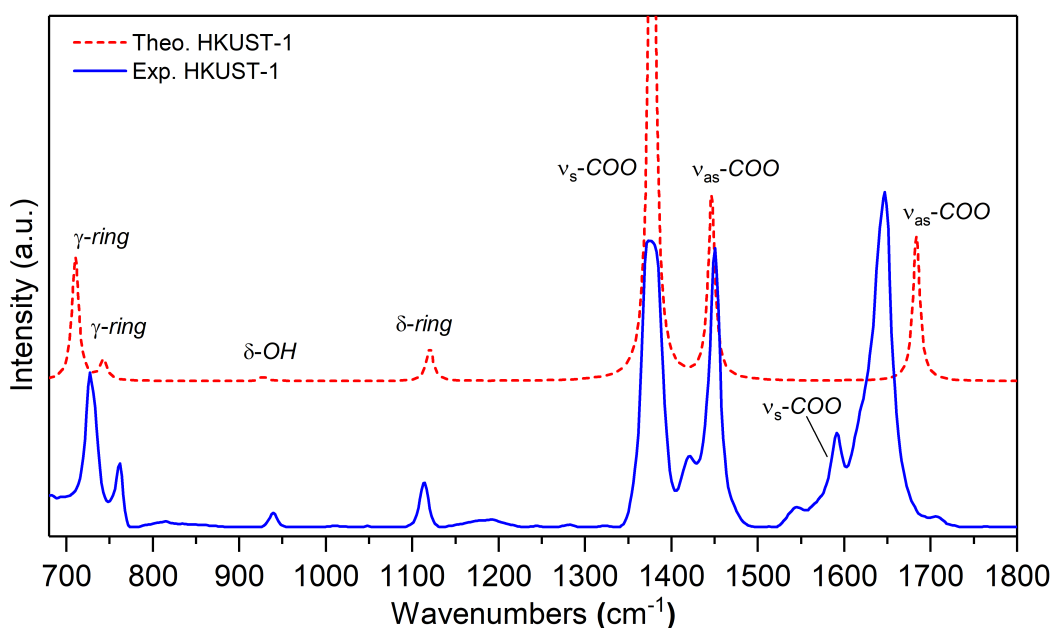


Figure S10. Band identification of HKUST-1 framework *via* density functional theory calculations. A scaling factor of 0.95 was applied to the theoretical spectra eliminate common shifts resulting from the *ab initio* calculations and match the frequencies against the experimental spectrum.

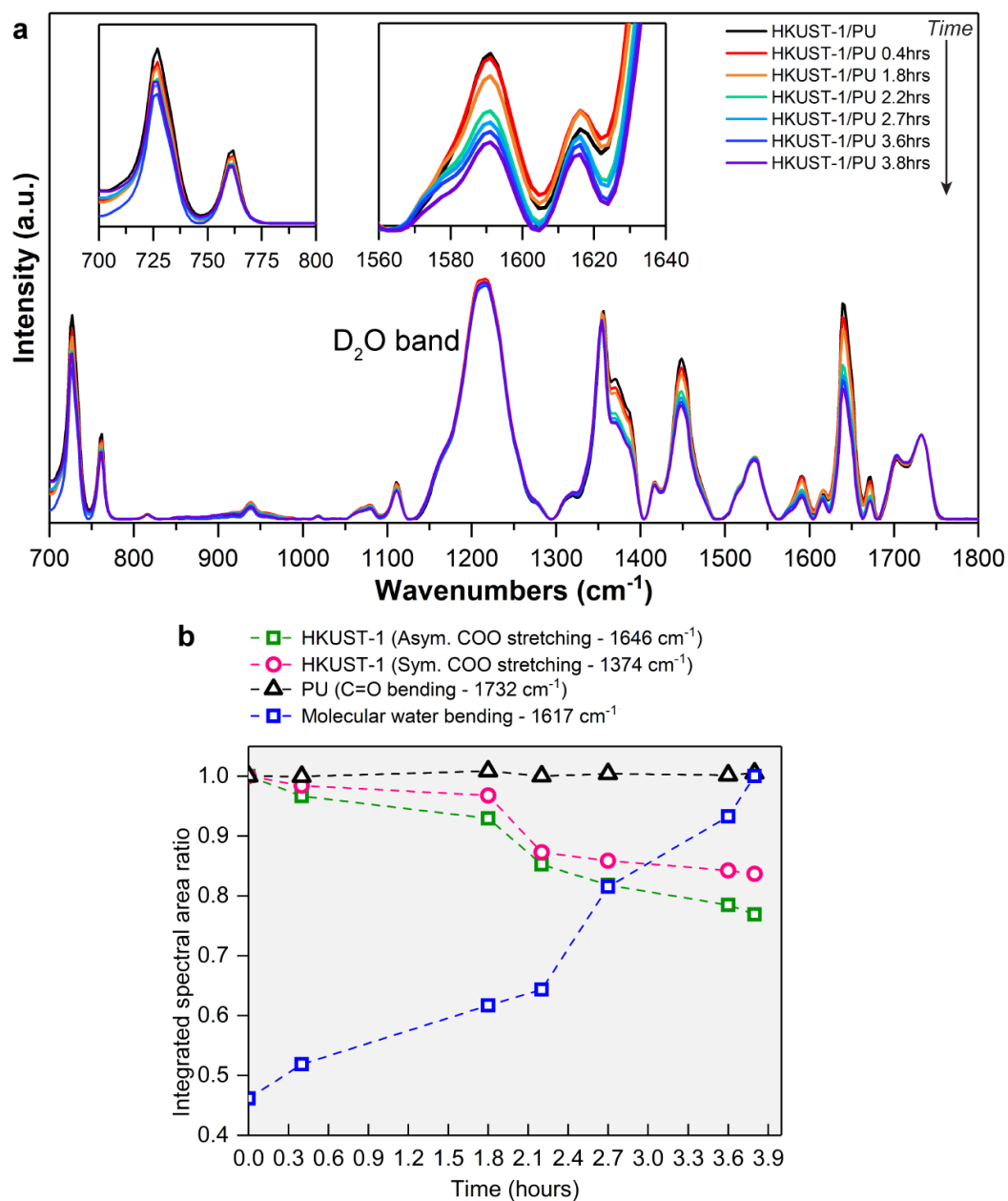


Figure S11. (a) Time evolution of HKUST-1/PU SR-microFTIR spectra collected during static fluid-cell experiments. (b) Evolution of integrated spectral area ratios of selected HKUST-1/PU peaks with time, upon coming into contact with water. Presented here are asymmetric and symmetric stretching modes of the carboxylate groups in HKUST-1, bending of molecular water, and PU C=O bending, used as the reference.

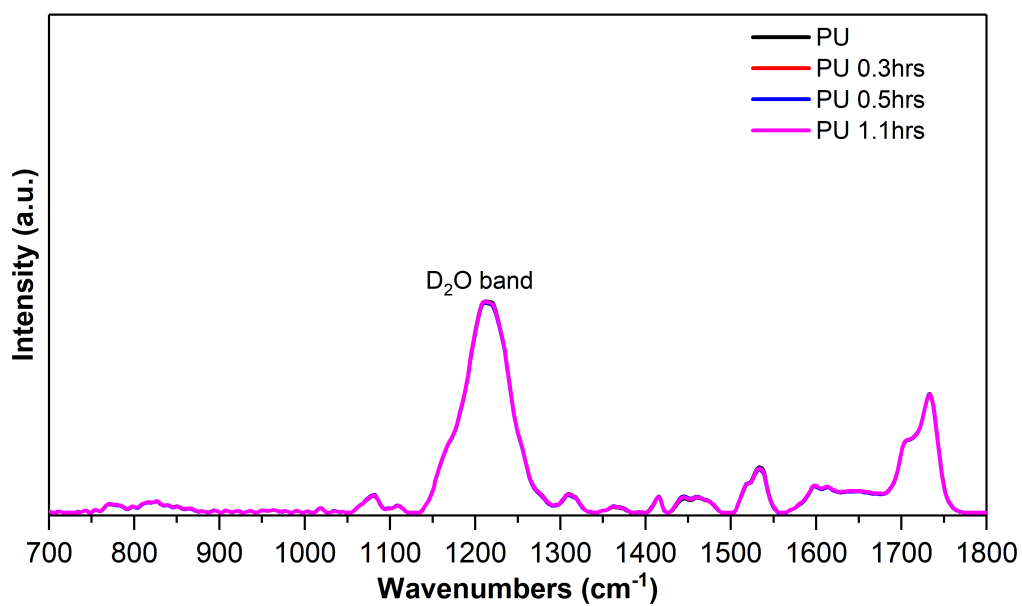


Figure S12. Time evolution of PU membrane SR-microFTIR spectra collected during static fluid-cell experiments, the overlapping data independent of time confirm the stability of the polymeric matrix subject to water.

6. Density functional theory (DFT) calculations

6.1. Adducts configuration

Four possible guest-host configurations of 5-FU encapsulated in the largest pore of HKUST-1 (*i.e.* 5-FU@HKUST-1), namely adducts A to D, as shown below (see Figure S12-S15), were investigated in the DFT calculations with the PBEsol0-3c method.¹⁹

In Figure S18a, the electrostatic potential mapped on top of a charge density isosurface for both HKUST-1 and 5-FU clearly shows that copper acts as a coordinatively unsaturated metal with a large positive region while oxygens in 5-FU molecule are surrounded by a strong negative region. The initial configurations for the four adducts have been created by matching the positive and negative regions of HKUST-1 and 5-FU and by considering the strong affinity between copper and oxygen. Therefore, a Cu—O bond was assumed as the dominant interaction in 5-FU@HKUST-1. Additionally, secondary interactions between NH groups of 5-FU and the negative regions around the carboxylate oxygens of the MOF could be envisaged, along with a less strong interaction between copper and fluorine. Furthermore, the Cu—Cu distances in the cage are compatible with the size of the drug molecule, thus making it possible to have the bridging geometries. Overall, the sum of these different interactions and chemical intuition have led to the four adducts shown in Figures S12-S15.

It is important to emphasize that the models herein proposed consider ideal drug loading within HKUST-1 pores, which can differ from the experimental sample with ~14 wt.% loading of 5-FU in HKUST-1.

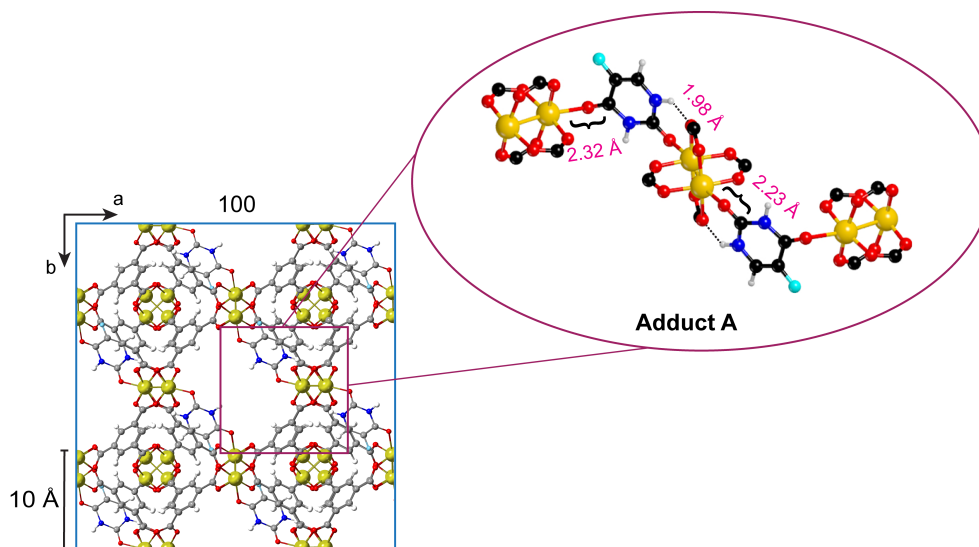


Figure S13. Adduct A configuration. In this adduct, 5-FU drug molecule (guest) interacts with two different paddle-wheels through its oxygen atoms. Hydrogen bonds are established between the N-H group of 5-FU and oxygen atoms in the carboxylate groups of the HKUST-1 (host) paddle-wheel. Note that in this case there are two molecules in the unit cell. Colour code: O in red, C in black, H in grey, Cu in yellow, N in navy blue, and F in turquoise.

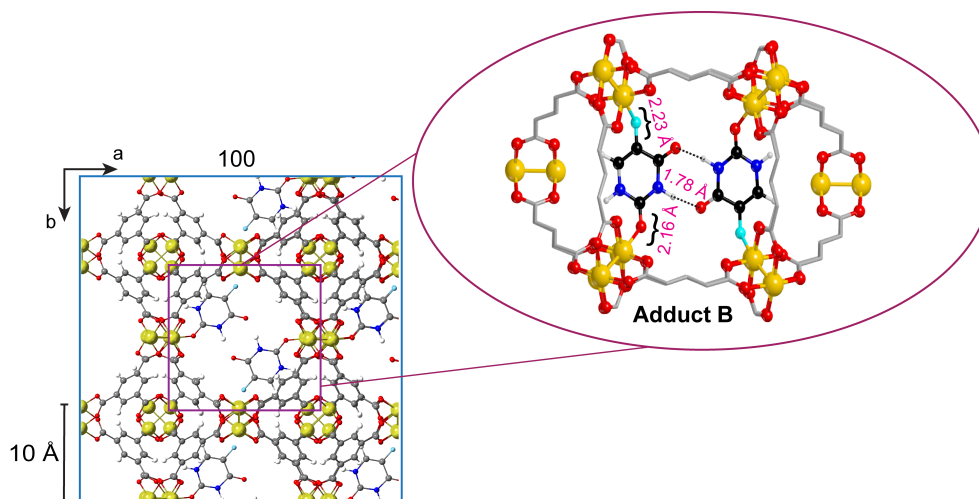


Figure S14. Adduct B configuration. In this adduct, the 5-FU guest is anchored to the adjacent paddle-wheels of the HKUST-1 (host) *via* its one of the oxygen atoms and fluorine, establishing NH---O hydrogen bonds with adjacent 5-FU molecules. Note that in this case there are two molecules in the unit cell. Colour code: O in red, C in grey, H in grey, Cu in yellow, N in navy blue, and F in turquoise.

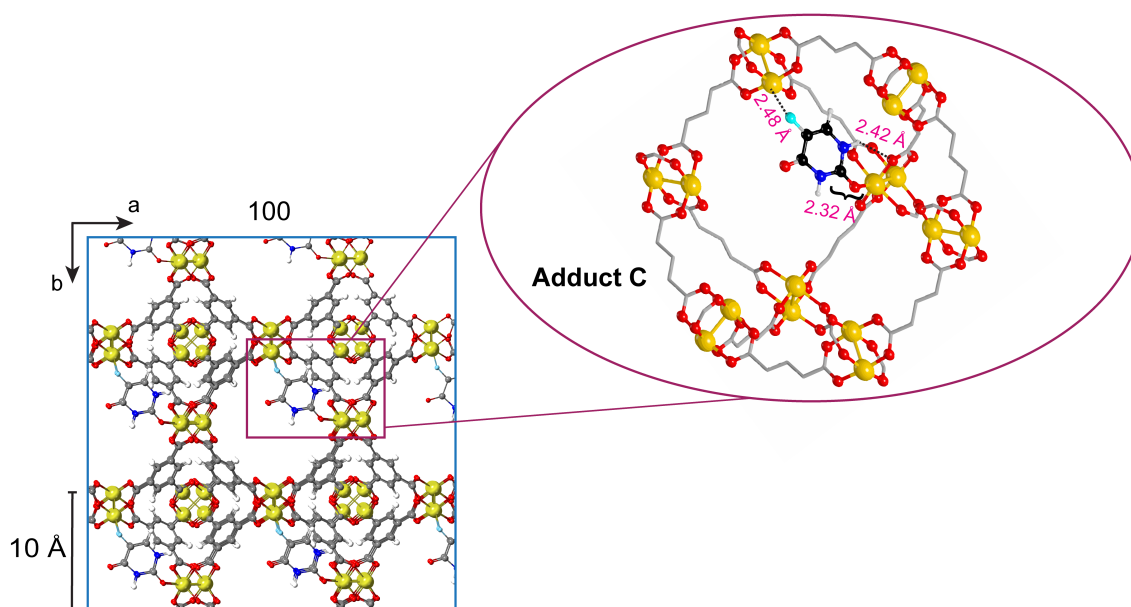


Figure S15. Adduct C configuration. 5-FU chelates two paddle-wheels *via* its oxygen and fluorine atoms. Note that in this case there is one molecule of 5-FU in the unit cell. Colour code: O in red, C in grey, H in grey, Cu in yellow, N in navy blue, and F in turquoise.

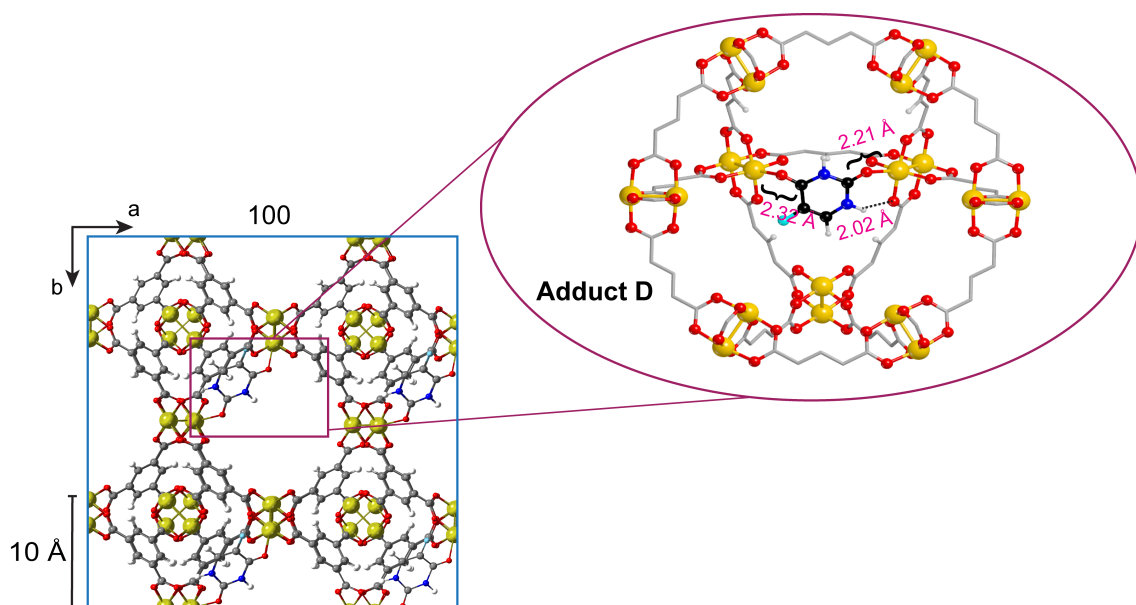


Figure S16. Adduct D configuration. In this configuration, 5-FU interacts with two different paddlewheels through its oxygen atoms. Note that this geometry is similar to adduct A but there is one molecule of 5-FU in the unit cell. Colour code: O in red, C in grey, H in grey, Cu in yellow, N in navy blue, and F in turquoise.

6.2. Binding energies and DFT model validation

Recently developed PBEsol0-3c is a cost-effective HF/DFT composite method combined with a double-zeta quality basis set that is expected to provide a good trade off between accuracy and cost.¹⁹ This has been demonstrated for inorganic solids, but it is also true for microporous materials as MOFs. As a check, here we benchmarked our new method by comparison with B3LYP-D3(ABC)/VTZP calculations that are more demanding. Figure S16 shows that computed binding energies for adducts A and D with both methods are very similar thus confirming the excellent accuracy of PBEsol0-3c.

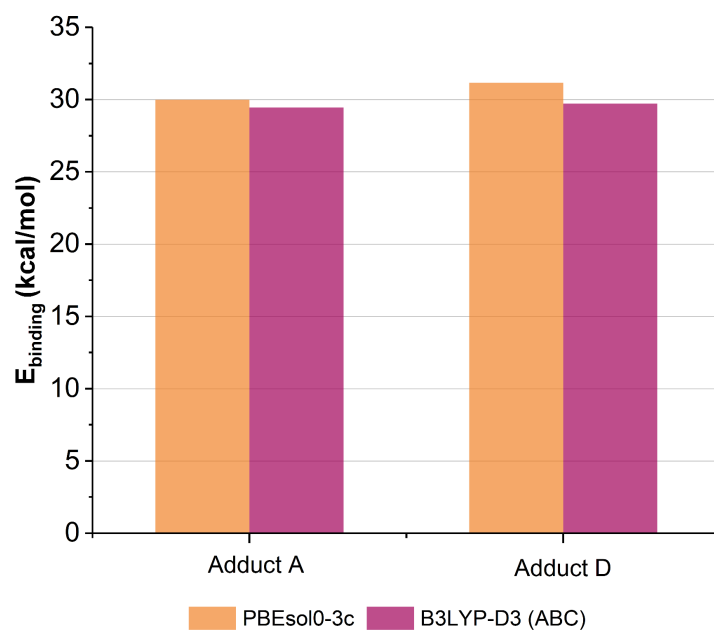


Figure S17. Comparison between binding energies calculated for adducts A and D configuration using PBEsol0-3c and B3LYP-D3(ABC) levels of theory and sol-def2-mSVP and Ahlrichs (VTZP) basis set, respectively. The good agreement between the computed binding energies applying both methods validating the new method developed and used in this work.

It is important to emphasize that the binding energies shown in Figure S17b should be interpreted according to the particularities of the adduct configurations, especially when comparing these binding energies with the water binding energy. Although, adducts A and B display two 5-FU molecules in each HKUST-1 pore, and adducts C and D are comprised of one 5-FU molecule per pore, all configurations show the adsorbate as bridged between two adjacent metal sites (see Figure S12-S15). In adducts A, B and D, for example, 5-FU is linked through oxygen-copper bonds while in adduct C the interaction involves one oxygen and the fluorine atom. It is worth noting that for the latter, not unexpectedly, the binding energy is the lowest one. As regards the competition with water, in adduct A, for example, the binding energy of each individual oxygen-copper bond might be considered to be ~ 15 kcal/mol, on average, very close the water binding energy of ~ 13.5 kcal/mol, and therefore highlighting the capability of water (D_2O and H_2O) to induce the release of the 5-FU molecules.

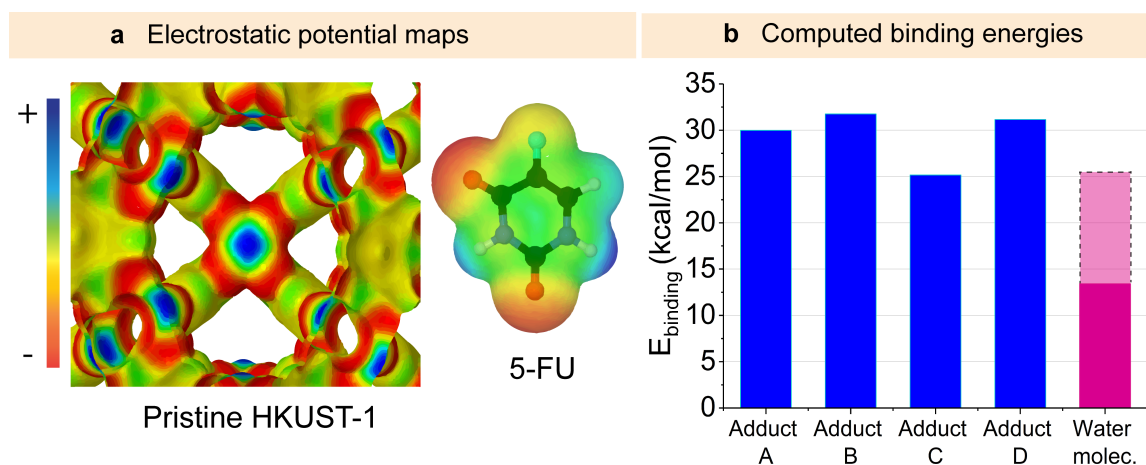


Figure S18. (a) Electrostatic potential maps of HKUST-1 (left) and 5-FU (right) supporting that 5-FU can strongly interact with the copper centres of HKUST-1 through its oxygen atoms generating both bridged and single site adducts. The interaction through the fluorine atom is possible but less likely due to the strength of the bond. (b) Binding energies of different adducts for the 5-FU - HKUST-1 interaction. The dashed line represent the binding energy relative to two water molecules, necessary for the release of the two 5-FU molecules encapsulated in the pores of adducts A and B.

6.3. Thermodynamic analysis to compute the enthalpy of adsorption

Table S4 gathers the different contributions needed to calculate the thermal correction to enthalpy and finally the enthalpy of adsorption for the different 5-FU@HKUST-1 adducts. In details, E_L is the electronic energy from DFT calculation, E_0 is the zero-point vibration energy and E_T is the thermal contribution to enthalpy. The latter term was obtained at $T = 298\text{K}$. From computed enthalpies the enthalpy of adsorption at 298 K was obtained as reported in Table S4. Results confirm that adduct C is the less favored configuration, while other adducts show similar ΔH s. In agreement with binding energies, also adsorption enthalpies show that two molecules can compete with 5-FU in the interaction with the metal site.

Table S4: Thermodynamic analysis of the different adduct configurations

	Adduct A	Adduct B	Adduct C	Adduct D	HKUST-1 + H ₂ O	HKUST-1 + D ₂ O
E_L (KJ/MOL)	-70994135	-70994150	-69649328	-69649353	-70703970	-70703970
E₀ (KJ/MOL)	2898.79	2898.42	2682.91	2683.84	3255.06	3047.48
E_T (KJ/MOL)	327.11	326.68	305.48	304.76	385.49	396.59
H (KJ/MOL)	-70990909	-70990925	-69646339	-69646364	-70700330	-70700526
ΔE (KCAL/MOL)	-30.01	-31.78	-25.24	-31.25	-13.41	-13.41
ΔH (KCAL/MOL)	-28.65	-30.51	-23.93	-29.88	-11.65	-11.90

6.4. Low energy vibrational bands *via* inelastic neutron scattering

Examination of the low energy vibrational bands, named the terahertz (THz) modes, offer additional insights on the agreement between the various adduct configurations (*i.e.* A-D) and the experimental 5-FU@HKUST-1 system. Using inelastic neutron scattering (INS) experimental data (previously reported by some of us)²⁰ and compare them to the theoretical INS spectra simulated from our DFT calculations, we can observe the possible coexistence of the adducts A-D. Contrasting the experimental spectra of pristine HKUST-1 and 5-FU@HKUST-1 (Figure S17a) we can observe the suppression of paddle-wheel vibrational modes due to the presence of 5-FU bound to the adjacent copper atoms. Similar effect can be noted in the theoretical spectra (Figure S17b), in which adduct D shows the most prominent effect in the suppression of HKUST-1 modes below 100 cm⁻¹, but analogous effect can also be observed in adducts A-C.

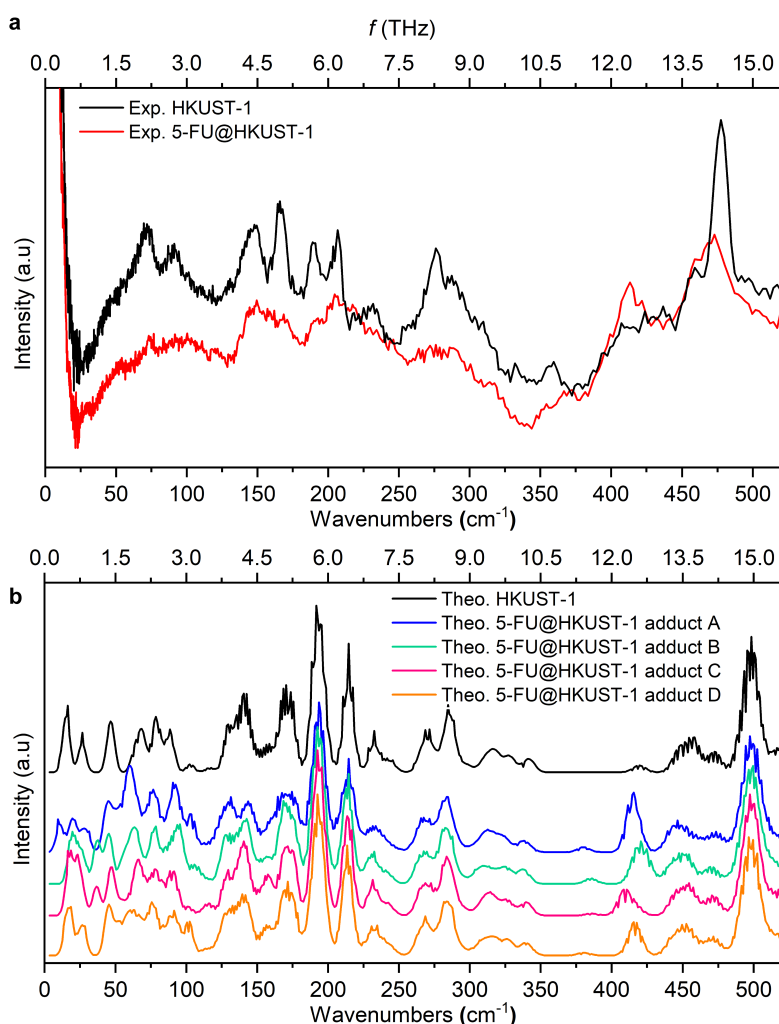


Figure S19. Inelastic neutron scattering (INS) spectra. Comparison between (a) experimental INS spectra of pristine HKUST-1, 5-FU@HKUST-1, and (b) theoretical INS spectra of pristine HKUST-1 and different adduct configurations (*i.e.* A-D)

7. Powder X-ray diffraction (PXRD) patterns

To perform the release of the 5-FU molecules from HKUST-1 for collection of diffraction data, 20 mg of the 5-FU@HKUST-1 were immersed in abundant methanol and constantly stirred at room temperature for a period of 72 hours. The material was recovered and washed by centrifugation twice with methanol (8000 rpm for 10 min) to guarantee complete removal of guest molecules present in the final composite sample.

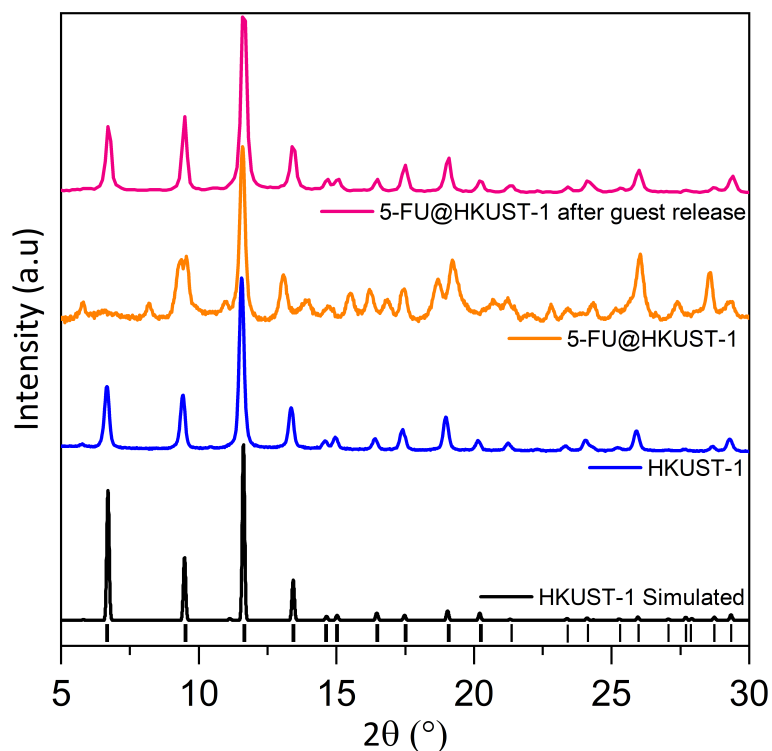


Figure S20. Diffraction patterns of manually ground HKUST-1 (blue) and its drug-loaded counterpart (orange). In pink is PXRD of 5-FU@HKUST-1 after the release of the 5-FU (guest) molecules. Recovery of cubic symmetry is clear when comparison is made between the diffraction pattern of the host framework obtained after guest release and simulated pattern of HKUST-1 (black).

8. Water accessibility in MOF/PU composites

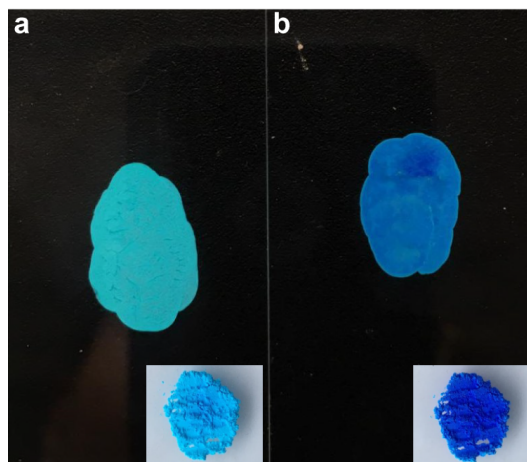


Figure S21. Change in color of membranes. HKUST-1/PU membrane (a) before and (b) after sample activation at 100 °C, and insets showing the corresponding powder samples. HKUST-1 framework presents a characteristic color switch from light blue (turquoise) to dark blue upon heating, linked to the change in coordination of the copper site. The color change observed in the composite membrane samples confirmed the accessibility of molecular water in and out of the polyurethane matrix.

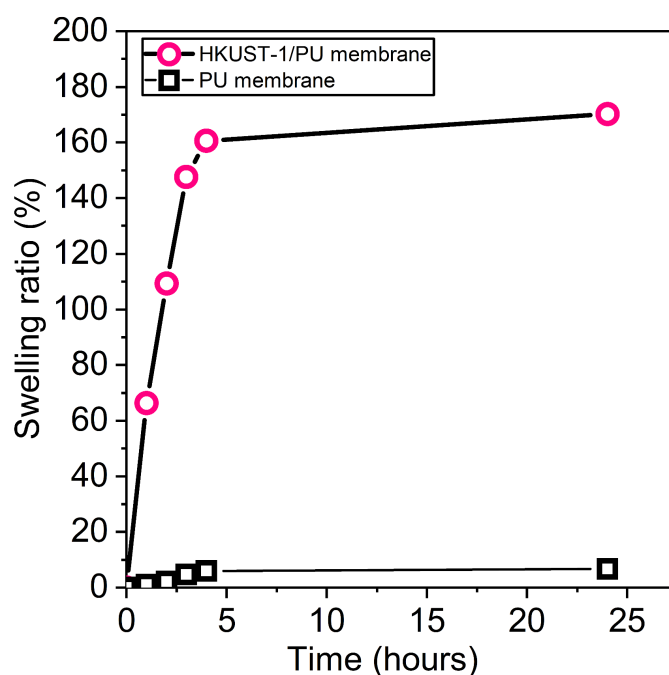


Figure S22. Swelling ratio of composites showcasing the superior absorption of water in HKUST-1/PU composite in comparison to a neat PU membrane.

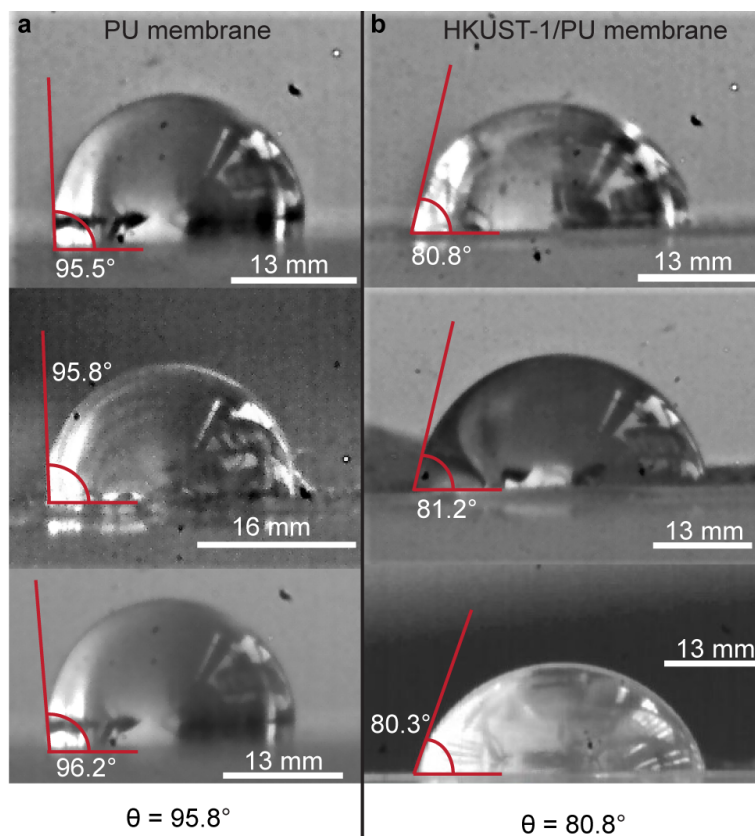


Figure S23. Contact angles of (a) PU membrane and (b) HKUST-1/PU membranes displaying the increase in the wettability of the membranes by the addition of HKUST-1 particles. Attempts were made to quantify the contact angle of HKUST-1 powder. However due to the hydrophilic character and high wettability of HKUST-1 powder, no water droplet was formed to allow the quantification of contact angle.

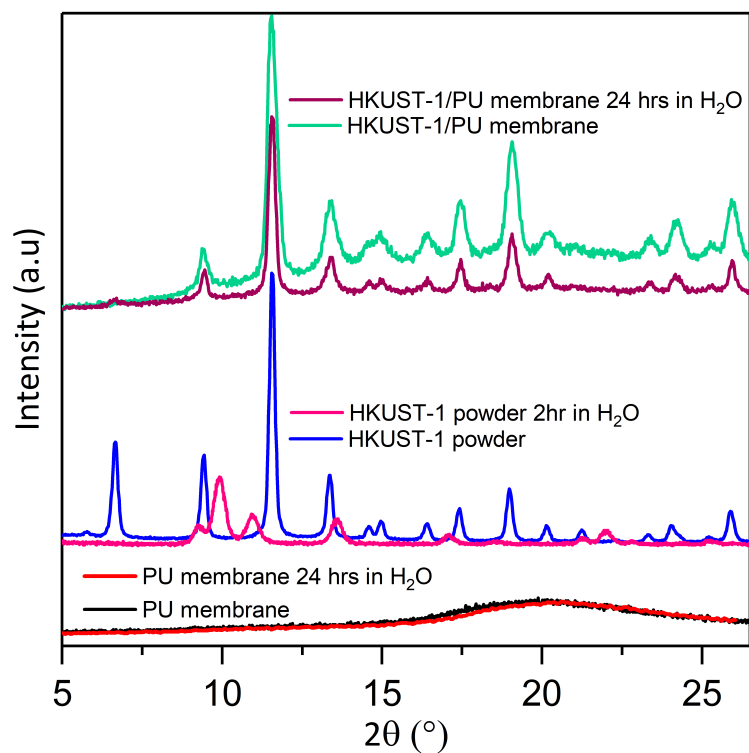


Figure S24. PXRD patterns of PU and HKUST-1/PU composite and HKUST-1 powder before and after immersion in water for 24 hours and 2 hours, respectively. The composites patterns show how the polymeric matrix can provide protection to the MOF, preventing hydrolysis. For HKUST-1 powder, the intensity of the diffraction peaks has decreased significantly after 2-hour immersion accompanied by emergence of new Bragg peaks suggesting phase transformation. In contrast, the diffraction pattern of HKUST-1/PU composite shows that it is considerably more stable even after 24 hours of immersion in water.

9. Analysis of synchrotron microFTIR data

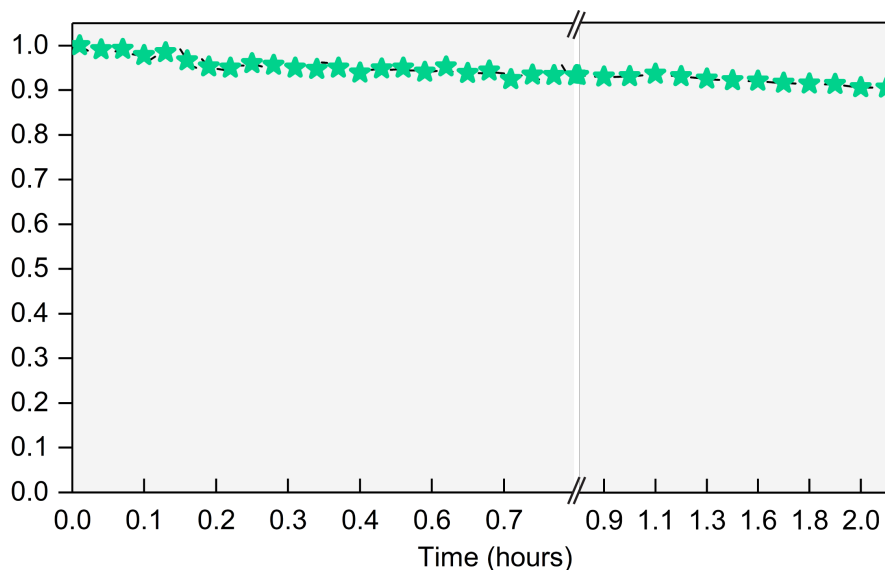


Figure S25. Integrated spectral area of 5-FU/PU peak (C-F stretching-1279 cm^{-1}) selected from spectra collected during the flow experiments.

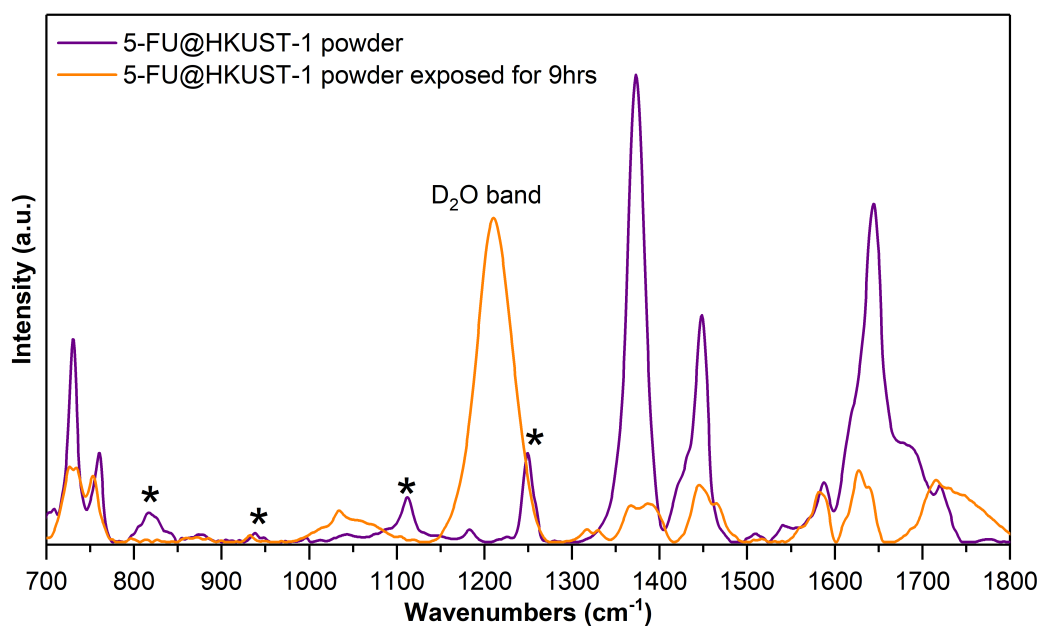


Figure S26. Comparison of 5-FU@HKUST-1 powder spectra before and after long exposure to moist environment. The spectra show the pronounced decomposition of the powder sample with degradation of main framework peaks as well as the disappearance of drug peaks, the latter marked by asterisks. The increase in intensity of the band at 1720 cm^{-1} indicates the presence of the acidic form of BTC.

References

1. Li, R.; Liu, S.; Tang, Q.; Wang, T.; Xie, Y.; Zhai, R., Encapsulation of 5-Fluorouracil in a Copper(II)-based Porous Metal-organic Framework: Drug Delivery and Inhibiting Human Spinal Cord Tumor Cells. *Z. Anorg. Allg. Chem.* **2018**, *644*, 317-321.
2. H. Zhou, E.; Wang, R.; Wu, J.; W. Qiu, S.; Q. Liu, J.; R. Zhong, H.; D. Zeng, H.; W. Xu, J.; C. Jin, J., A 3D polyhedral metal-organic framework as drug carrier for controllable release. *B. Chem. Soc. Ethiopia* **2018**, *31*, 457-463.
3. Li, Y.; Li, X.; Guan, Q.; Zhang, C.; Xu, T.; Dong, Y.; Bai, X.; Zhang, W., Strategy for chemotherapeutic delivery using a nanosized porous metal-organic framework with a central composite design. *Int. J. Nanomedicine* **2017**, *12*, 1465-1474.
4. Ho, P. H.; Salles, F.; Di Renzo, F.; Trens, P., One-pot synthesis of 5-FU@ZIF-8 and ibuprofen@ZIF-8 nanoparticles. *Inorganica Chim. Acta* **2020**, *500*.
5. Li, H.-T.; Song, S.-J.; Pei, X.-R.; Lu, D.-B., A InIII-MOF with Imidazole Decorated Pores as 5-Fu Delivery System to Inhibit Colon Cancer Cells Proliferation and Induce Cell Apoptosis in vitro and in vivo. *Z. Anorg. Allg. Chem.* **2019**, *645*, 801-809.
6. Wei, D.; Xin, Y.; Rong, Y.; Li, Y.; Zhang, C.; Chen, Q.; Qin, S.; Wang, W.; Hao, Y., A Mesoporous Gd-MOF with Lewis Basic Sites for 5-Fu Delivery and Inhibition of Human Lung Cancer Cells In Vivo and In Vitro. *J. Inorg. Organ. Polym. Mat.* **2019**, *6*, 1550-1557.
7. Song, B.-H.; Ding, X.; Zhang, Z.-F.; An, G.-F., Efficient drug delivery of 5-fluorouracil by a biocompatible Zn-metal-organic framework nanostructure and anti-liver cancer activity study. *J. Iran. Chem. Soc.* **2018**, *16*, 333-340.
8. Zhao, L.-C.; Tang, M.; Zhang, Q.-H.; Hu, Z.-Y.; Gao, H.-W.; Liao, X.-Y.; Wang, G.; Leng, J., Fabrication of a Porous Metal-Organic Framework with Polar Channels for 5-Fu Delivery and Inhibiting Human Osteosarcoma Cells. *J. Chem.* **2018**, *7*, 5294-5301.
9. Du, P.-Y.; Gu, W.; Liu, X., A three-dimensional Nd(iii)-based metal-organic framework as a smart drug carrier. *New J. Chem.* **2016**, *40*, 9017-9020.
10. Han, Y.; Liu, W.; Huang, J.; Qiu, S.; Zhong, H.; Liu, D.; Liu, J., Cyclodextrin-Based Metal-Organic Frameworks (CD-MOFs) in Pharmaceuticals and Biomedicine. *Pharmaceutics* **2018**, *10*, 271 .
11. Nguyễn Thị Hoài Phương, N. Đ. H., Investigation in Loading 5-Fluorouracil Ability of Iron-Organic Frameworks. *Vietnam J. Sci. Technol.* **2018**, *56*, 219-227.
12. Xing, K.; Fan, R.; Wang, F.; Nie, H.; Du, X.; Gai, S.; Wang, P.; Yang, Y., Dual-Stimulus-Triggered Programmable Drug Release and Luminescent Ratiometric pH Sensing from Chemically Stable Biocompatible Zinc Metal-Organic Framework. *Acs Appl. Mater. Inter.* **2018**, *10*, 22746-22756.
13. Tummala, S.; Satish Kumar, M. N.; Prakash, A., Formulation and characterization of 5-Fluorouracil enteric coated nanoparticles for sustained and localized release in treating colorectal cancer. *Saudi Pharm. J.* **2015**, *23*, 308-314.
14. Tıǧlı Aydın, R. S.; Pulat, M., 5-Fluorouracil Encapsulated Chitosan Nanoparticles for pH-Stimulated Drug Delivery: Evaluation of Controlled Release Kinetics. *J. Nanomaterials* **2012**, *2012*, 1-10
15. Arias, J. L., Novel strategies to improve the anticancer action of 5-fluorouracil by using drug delivery systems. *Molecules* **2008**, *13*, 2340-69.
16. Rastogi, V. K.; Palafox, M. A., Vibrational spectra, tautomerism and thermodynamics of anticarcinogenic drug: 5-fluorouracil. *Spectrochim. Acta A. Mol. Biomol. Spectrosc.* **2011**, *79*, 970-7.
17. Wang, F. C.; Feve, M.; Lam, T. M.; Pascault, J.-P., FTIR analysis of hydrogen bonding in amorphous linear aromatic polyurethanes. I. Influence of temperature. *J. Polym. Sci. Pol. Phys.* **1994**, *32*, 1305-1313.
18. Wang, F. C.; Feve, M.; Lam, T. M.; Pascault, J.-P., FTIR analysis of hydrogen bonding in amorphous linear aromatic polyurethanes. II. Influence of styrene solvent. *J. Polym. Sci. Pol. Phys.* **1994**, *32*, 1315-1320.
19. Dona, L.; Brandenburg, J. G.; Civalleri, B., Extending and assessing composite electronic structure methods to the solid state. *J Chem Phys* **2019**, *151*, 121101.
20. Souza, B. E.; Rudic, S.; Titov, K.; Babal, A. S.; Taylor, J. D.; Tan, J. C., Guest-host interactions of nanoconfined anti-cancer drug in metal-organic framework exposed by terahertz dynamics. *Chem. Commun.* **2019**, *55*, 3868-3871.